HHS Public Access

Author manuscript

*Nat Biotechnol*. Author manuscript; available in PMC 2019 August 25.

Published in final edited form as:

*Nat Biotechnol*. 2019 March ; 37(3): 267–275. doi:10.1038/s41587-019-0035-0.

# NFIA is a gliogenic switch enabling rapid derivation of functional human astrocytes from pluripotent stem cells

**Jason Tchieu**[1,2], **Elizabeth L. Calder**[1,2], **Sudha R. Guttikonda**[1,2,3], **Eveline M. Gutzwiller**[1,2], **Kelly A. Aromolaran**[4], **Julius A. Steinbeck**[1,2], **Peter A. Goldstein**[4], and **Lorenz Studer**[1,2,*]

[1]The Center for Stem Cell Biology

[2]Developmental Biology Program, Sloan-Kettering Institute for Cancer Research

[3]Weill Cornell/Rockefeller/Sloan Kettering Tri-Institutional MD-PhD Program, New York, NY 10065 USA.

[4]Department of Anesthesiology, Weill Cornell Medicine, 1300 York Ave, New York, NY 10065, USA

## Abstract

The mechanistic basis of gliogenesis, which occurs late in human development, is poorly understood. Here we identify nuclear factor IA (NFIA) as a molecular switch for inducing human glial competency. Transient expression of NFIA is sufficient to trigger glial competency of human pluripotent stem cell-derived neural stem cells within 5 days and to convert these cells into astrocytes in the presence of glial-promoting factors, compared to 3–6 months using current protocols. NFIA-induced astrocytes promote synaptogenesis, exhibit neuroprotective properties, display calcium transients in response to appropriate stimuli, and engraft in the adult mouse brain. Differentiation involves rapid but reversible chromatin remodeling, GFAP promoter demethylation, and a striking lengthening of the G1 cell cycle phase. Genetic or pharmacological manipulation of G1 length partially mimics NFIA function. We use the approach to generate astrocytes with region-specific or reactive features. Our study defines key mechanisms of the gliogenic switch and enables the rapid production of human astrocytes for disease modeling and regenerative medicine.

Astrocytes are the most abundant glial cell type in the human brain, and their dysfunction is a driver in the pathogenesis of both neurodevelopmental and neurodegenerative disorders[1].



*Correspondence to: Dr. Lorenz Studer, The Center for Stem Cell Biology, Developmental Biology Program, Memorial Sloan-Kettering Cancer Center, 1275 York Ave, Box 256, New York, NY 10065, Phone: 212-639-6126, Fax: 212-717-3642, studerl@mskcc.org.

AUTHOR CONTRIBUTIONS

J.T.: Conception, study design, data analysis and interpretation, writing of manuscript, bioinformatics, development and execution of directed differentiation strategies from hPSCs, generation of LTNSCs, cell cycle analysis, calcium imaging. E.L.C.: Maintenance of hPSCs, directed differentiation of spinal cord progenitors. S.R.G.: Cell cycle analysis, astrocyte activation assays. E.M.G.: Transplantation studies, data analysis. K.A.A. and P.A.G.: Electrophysiology and assessment of neuronal maturation. J.A.S.: Generation of LTNSCs and calcium imaging. L.S.: Conception, study design, data analysis and interpretation, writing of manuscript.

COMPETING FINANCIAL INTERESTS

The authors declare no competing financial interests

The study of human astrocytes has been challenging owing to their limited availability and regional heterogeneity[2]. Astrocytes are derived from late neural stem cells (NSCs). During early development, NSCs are fate-restricted to exclusively produce neurons, while at later stages they undergo a switch from neurogenic to gliogenic competency, resulting in progressive production of astrocytes and oligodendrocytes[3]. The molecular nature of the gliogenic switch has remained elusive, and its timing varies across species, from 7 days in the mouse to 6–9 months in humans[4]. These species-specific differences are reflected in methods for *in vitro* differentiation of PSCs, with the derivation of human astrocytes requiring 3–6 months[5,6]. Differentiation into NSCs results in a long neurogenic phase followed by a late gliogenic switch, mimicking the time-line of human glial development. Previous studies report the need to culture hPSC-derived NSCs for up to 24 weeks before obtaining large populations of functional astrocytes upon differentiation[7,8]. Following extended culture, the gliogenic switch occurs spontaneously, but the molecular mechanism underlying the switch remains unclear[9]. The protracted time for acquiring glial competency presents a roadblock in basic and translational studies of human astrocytes.

To monitor when astrocytes develop during hPSC differentiation, we generated a knock-in reporter line targeting the aquaporin-4 (AQP4) locus with a nuclear green fluorescent protein (H2B-GFP) (Supplemental Fig. 1). Previous strategies for generating astrocytes from hPSCs include the exposure of factors such as LIF, CNTF, BMP, or serum to NSCs to trigger glial differentiation[10,11]. The onset of glial differentiation was moderately accelerated in NSCs treated with serum (Supplemental Fig. 2), and we tested whether such acceleration was correlated with changes in the expression of candidate factors including NFIA (Fig. 1A) previously implicated in glial fate acquistion[12,13,14,15,16].

To directly test whether these genes impact glial competency or differentiation, we used a homogeneous and stable neurogenic NSC population termed long term human embryonic stem cell derived neural stem cells (lt-hESNSCs[17], referred to as LTNSCs in this study). Unlike NSCs, LTNSCs do not spontaneously undergo the gliogenic switch upon long-term culture but remain in the neurogenic phase[18] (Supplemental Fig. 3), making them ideal for identifying factors involved in the gliogenic switch. While knockdown of *LIN28B* did not show any obvious effect, overexpression of *NFIA* profoundly altered LTNSC morphology (Supplemental Fig. 4A, C) and correlated with expression of NFIA protein and CD44[19], a marker of glial competency, although it did not result in GFAP-positive cells (Fig. 1B). A subset of the NFIA-expressing cells activated the *AQP4-H2B-GFP* reporter (Supplemental Fig. 4B). We hypothesized that the overexpression of NFIA triggers glial competency but blocks differentiation toward astrocytes. We performed a time course study in which LTNSCs were cultured in the presence (dox+) or absence (dox-) of NFIA expression. After 5 days, cells were switched to (dox-) either in a glial promoting condition (+LIF) or in NSC maintenance medium (+EGF/FGF2). Notably, continued expression of NFIA (dox+) prevented LTNSCs from expressing GFAP even in the presence of LIF (Fig. 1C (dox+)). In contrast, removal of doxycycline led to a decline in NFIA expression for both conditions, but GFAP expression was strongly induced only in the (+LIF) group and only after NFIA was sufficiently downregulated (Fig. 1C). We found that LIF was most efficient in generating GFAP-positive cells and in activating the AQP4-H2B-GFP reporter compared to other glial differentiation factors (Supplemental Fig. 5A, B). These results show that glial competency

in neurogenic human NSCs can be achieved in 5 days by transient expression of NFIA compared with 90–180 days using current protocols (Supplemental Fig. 6A).

We determined the timing and efficiency of astrocyte generation using NFIA. While there was a robust increase in GFAP expression, not all cells were immediately immunoreactive to GFAP. We used intracellular FACS to determine the absolute numbers of GFAP-positive and CD44-positive cells at different passages after NFIA induction (Supplemental Fig. 6B). We achieved >60% GFAP-expressing cells by 56 days of culture and nearly 100% GFAP-positive cells after 77 days (Fig. 1D, E). We determined that the success of astrocyte generation was dependent on the transduction efficiency of the NFIA virus in NSCs. To further improve the efficiency of generating astrocytes from hPSCs (Supplemental Fig. 6C), we generated an inducible NFIA hPSC-line (NFIA-hPSC, Supplemental Fig. 7A). NFIA is not expressed in hPSCs and was induced by dox treatment to identify properly targeted clones (Supplemental Fig. 7B). Western blot analysis showed NFIA levels were higher in the inducible line compared to transduced LTNSCs (Supplemental Fig. 7C).

To determine efficiency, we differentiated the inducible NFIA-hPSCs into cortical NSCs (Supplemental Fig. 6C) and induced NFIA for 10 days (Supplemental Fig. 7D, E). In this time, 65% of the cells became CD44 positive. LIF treatment for 15 days led to 42% of the cells expressing GFAP (Supplemental Fig. 7F, G, H). Immunostaining of the resulting cells showed expression of S100β and GFAP and loss of the proliferation marker KI-67 (Supplemental Fig. 7I). Finally, to test the suitability of the protocol for disease modeling, we differentiated isogenic control and patient-specific iPSCs harboring a mutation in the SOD1 gene (A4V)[20] toward cortical versus spinal cord progenitor identity[18,21] and confirmed their distinct antero-posterior marker expression (Supplemental Fig. 8A, B). By infecting the progenitors with NFIA, we observed the expression of GFAP-positive cells by 6–7 days of differentiation (Supplemental Fig. 8C) resulting in regionally distinct astrocytes (Supplemental Fig. 8D). This reaffirms that NFIA-induction is a robust strategy to generate astrocytes of specific regional identity across control and disease hPSCs.

The cells derived from NFIA-induced NSCs yielded astrocytes with complex morphologies (Fig. 1F) that expressed a panel of genes representing astrocyte identity (Fig. 1G). To further determine whether NFIA-induced astrocytes matched astrocytes observed *in vivo*, we performed gene expression profiling (Fig. 1H). A broad set of RNAseq data from NFIA-induced astrocytes at various stages of differentiation was compared to published datasets from hPSC-derived astrocytes from conventional, protracted differentiation conditions[6], hPSC-derived astrocytes from serum exposure[10], and astrocytes from primary human fetal tissue[22]. Initial comparison of the samples demonstrated high correlation between the NFIA-induced astrocytes and astrocytes generated using protracted methods. This is in contrast with hPSC-derived astrocytes using a serum method of differentiation (Supplemental Fig. 9A, B). We performed a comparative analysis of our dataset with one that encompasses freshly isolated fetal and adult astrocytes as well as a range of additional primary lineages isolated from human cortex[2] and across a set of astrocyte-specific genes shared among three independent astrocyte studies[23-25]. This analysis showed close correlation between NFIA-induced astrocytes and fetal astrocytes (Fig. 1H **and** Supplemental Fig. 9C, D, Supplemental Table 1).

We examined the functionality of NFIA-induced astrocytes. Astrocytes play critical roles during CNS development, including neuronal maturation[26], maintenance of metabolic homeostasis, and regulation of inflammation in the nervous system[27]. Several genes associated with the formation of functional synapses[28] were upregulated (Supplemental Fig. 9E) suggesting that these cells exhibit functional properties in neuronal maturation. Immature neurons co-cultured in the presence of NFIA-induced astrocytes showed evidence of accelerated maturation by the increased expression and appearance of punctate SYN1 (synapsin-I) (Fig. 2A) and upregulation of an active zone marker MUNC13.1[29] (Fig. 2B). Additionally, the co-localization of pre- and postsynaptic markers, such as SYN1 and HOMER, indicated the formation of structural synapses (Fig. 2C **and** Supplemental Fig. 10). NFIA-induced astrocytes also promoted neuronal survival when subjected to glutamate excitotoxicity (Supplemental Fig. 11)[30]. Notably, upon cytokine treatment, we could trigger the upregulation of reactive astrocyte (A1) specific transcripts (Supplemental Fig. 12A, B) and complement (C3) secretion[1,31] (Fig. 2D). Morphologically, astrocytes cultured at different passages appear to transition from large flat cells to cells with long and complex processes (Supplemental Fig. 13A).

NFIA-induced astrocytes can be stimulated to elicit calcium transients[32] in response to specific stimuli. Commercially available primary astrocytes isolated from human fetal brains (19–23 pcw) displayed morphologies similar to NFIA-induced astrocytes; however, only few cells responded to the stimuli (Supplemental Fig. 14G). In contrast, NFIA-induced astrocytes responded robustly to KCl and ATP (Fig. 2E **and** Supplemental Fig. 14A-D) with increasing ATP responsiveness over time (Supplemental Figure 14H). When in co-culture with hPSC-derived neurons, NFIA-induced astrocytes adopted a more ramified appearance (Supplemental Fig. 13B) and showed increased *AQP4-H2B-GFP* signal (Supplemental Fig. 14F), and the response to ATP increased by 2-fold (Fig. 2G). In addition, the magnitude of the glutamate response was enhanced, suggesting a synergistic interaction between the two cell types in mutually driving both glial and neuronal maturation (Fig. 2F, G).

We tested whether NFIA-induced astrocytes promoted the functional maturation of immature hPSC-derived cortical neurons (Supplemental Fig. 15A). Whole cell recordings from cortical neurons and cortical neurons cultured with NFIA-induced astrocytes revealed a resting membrane potential of −56.1 ± 2.5 mV and −72 ± 2.2 mV, respectively (Fig. 2H). Similarly, the input resistance of cortical neurons significantly decreased upon co-culture with NFIA-induced astrocytes, further suggesting a more mature phenotype in the presence of astrocytes (Fig. 2I). To monitor the impact on synaptic maturation, we recorded basal spontaneous miniature excitatory postsynaptic currents (mEPSCs) (Supplemental Fig. 15B) and observed a decrease in inter-event interval (Supplemental Fig. 15C) and an increase in mEPSC frequency from 0.22 ± 0.01 to 0.39 ± 0.02 Hz (Fig. 2J) in neurons co-cultured with glia, indicating increased synaptic activity. We also observed an increase in amplitude (12.5 ± 0.2 vs. 13.6 ± 0.2 pA) (Fig. 2K) and time course of decay (6.7 ± 0.3 vs. 7.6 ± 0.3 ms) (Supplemental Fig. 15D) in mEPSCs from neurons in the presence of glia.

Finally, we transplanted neurogenic NSCs, NFIA-induced glial-competent NSCs or astrocytes in the adult mouse cortex and corpus callosum. At 2 weeks post-transplantation, the glial progenitors migrated extensively from the graft core along white matter tracts (Fig.

2L) whereas neurogenic NSCs resulted in a dense graft composed largely of neurons (Supplemental Fig. 16A-C). The grafted NFIA-induced cells maintained expression of AQP4-H2B-GFP as well as GFAP and displayed morphological features characteristic of human astrocytes by 6 weeks post-transplantation (Fig. 2M, Supplemental Fig. 16D-F), with complex morphologies and extensive GFAP-positive projections spanning multiple cortical regions[33] (Supplemental Fig. 16G).

The above *in vitro* and *in vivo* data demonstrate that transient NFIA expression generates functional, region-specific human astrocytes on demand at high speed and efficiency. Furthermore, they show that NFIA is a key component of the molecular switch for triggering human glial competency. To explore the NFIA mechanism of action, we returned to our initial observation that transient NFIA expression triggers glial competency but does not induce endogenous NFIA expression (**refer to** Fig. 1C). Once doxycycline is removed and cells are maintained in NSC media, they lose glial competency (Fig. 3A) and return to a neurogenic state (Fig. 3B). We performed a time course analysis of ectopic NFIA expression followed by sorting for CD44-positive cells and replating in the absence of dox (dox-) (Fig. 3C). We confirmed that NFIA expression is lost after 3 days of culture without doxycycline (d9) (Fig. 3D). Based on gene expression data by RNAseq, we observed three major clusters among the samples throughout the time course (Fig. 3E, Supplemental Table 2). Of these, neuroepithelial stage NSCs, LTNSCs (d0), and samples reverted to dox- clustered together, supporting the notion that the NFIA pulse cannot maintain glial competency upon NFIA withdrawal.

Notably, NFIA expression for 6 days induced a chromatin accessibility landscape similar to that of hPSC-derived astrocytes (d200) or glial-competent NSCs (d80) (Fig. 3F). Differential chromatin accessibility was associated with a clear shift in the enrichment of transcription factor binding motifs. *SOX* and *ZNF354C* motifs were enriched in the d0 (dox-) and the d12 (reverse) conditions, and *AP-1, NFIX* and *NFI* half site motifs were highly enriched in the d6 (dox+) and astrocyte conditions (Supplemental Fig. 17). Unexpectedly, the *GFAP* promoter did not show differential accessibility (Fig. 3G, bottom) even though our previous experiments showed robust induction of *GFAP* in the presence of LIF after only a short pulse of *NFIA* but not with LIF treatment alone. However, bisulfite sequencing of the GFAP promoter consistently highlighted one CpG in the *GFAP* promoter with a loss of methylation in CD44-positive cells (Fig. 3H) and was similarly unmethylated in astrocytes but not in LTNSCs. This CpG matches a *STAT3* binding site[34] that is predicted to inhibit STAT3 binding when methylated. These data suggest that NFIA induces glial competency by multiple modes, including the regulation of chromatin accessibility and DNA demethylation.

We examined the differential gene expression programs induced by NFIA overexpression and after NFIA withdrawal in LTNSCs using RNAseq and DAVID functional annotation analysis software[35]. Hierarchical clustering of all differentially expressed genes during the time course displayed three major clusters with distinct temporal profiles (Fig. 4A, labeled I, II and III). Cluster I includes genes associated with glial differentiation (Supplemental Fig. 18A). Genes associated with oligodendrocyte differentiation were absent from Cluster I. Cluster II comprises genes directly affected by *NFIA* expression and that are rapidly lost upon *NFIA* reduction (Supplemental Fig. 18B). Cluster III encompasses genes

downregulated upon expression of *NFIA*. These genes were specifically enriched for cell cycle–related processes, such as cell division, chromosome segregation, DNA repair and replication (Fig. 4B). *NFIA* triggered a negative regulation of cell cycle–specific genes (Fig. 4C), which was reversed after *NFIA* removal (Fig. 4D, Supplemental Fig. 19A).

We studied whether functional changes in cell cycle progression were the key to acquisition of glial competency. A large proportion of cells accumulated in G1 following *NFIA* expression in LTNSCs (Fig. 4E). Although expression of *CCNA1* was upregulated with NFIA (Supplemental Fig. 19B), there was a striking decrease in CCNA1 protein and marked increase in CDKN1A (p21) (Fig. 4F). Progressive lengthening of G1 was reported as a characteristic feature of the developing rodent cortex[36] from early embryonic (neurogenic) to later fetal (gliogenic) stages—a transition during which hPSC-derived NSCs show progressive endogenous expression of NFIA (Supplemental Fig. 20A). To directly measure cell-cycle lengthening, we used the FUCCI-O vector to determine the time cells spent in G1[37]. Time-lapse analysis demonstrated that a large proportion of cells showed lengthening of the G1 phase in the (dox+) condition compared to uninduced cells (Movie S1 and S2; Supplemental Fig. 20B). We also explored whether reducing *NFIA* levels would result in a more moderate G1 length compatible with acquiring glial fate. Indeed, when we titrated *NFIA* levels by varying dox concentrations, the percentage of cells in G1 gradually decreased along with reduced dox levels, and *GFAP* expression was induced only at lower dox concentrations in the presence of LIF (Supplemental Fig. 20D, E).

To examine whether pharmacological modulation of the cell cycle in the absence of NFIA expression is sufficient to trigger the gliogenic switch, we treated cells with Olomoucine (Olo), a small molecule known to lengthen G1 timing *in vitro*[38]. Treatment of LTNSCs with Olo increased the percentage of cells in G1 (Supplemental Fig. 21A) but did not immediately activate expression of glial competency genes (Supplemental Fig. 21B). However, when Olo-treated LTNSCs were either maintained or induced to differentiate for an additional 12 days, we detected increased expression of glial competency genes and GFAP-positive cells (Supplemental Fig. 21C, D). Conversely, we knocked down *FZR1*(*CDH1*), which shortens the G1 cell-cycle phase[39,40]. shRNA constructs targeting *FZR1* showed efficient knockdown of the transcript (Fig. 4G), did not affect levels of NFIA expression, and decreased the percentage of cells in G1 (Fig. 4H). Indeed, the knockdown of *FZR1* partially prevented NFIA-mediated induction of *CD44* and *GFAP* expression (Fig. 4I, J).

Finally, we explored the identity of candidate upstream activators of *NFIA*. Transforming growth factor beta (TGFβ) signaling has been implicated in timing of cell fate decisions in the spinal cord[41] and is known to modulate G1 arrest[42]. TGFβ1 treatment of neurogenic NSCs induced the expression of NFIA (Fig. 4K) and enriched for cells in the G1 phase of the cell cycle (Fig. 4L). We treated neurogenic NSCs with TGFβ1 followed by culture in LIF-containing medium for 2 weeks, which resulted in the appearance of GFAP+ cells (Fig. 4M). These results indicate that TGFβ1-mediated induction of NFIA and concomitant G1 lengthening are sufficient to trigger gliogenesis. However, the resulting levels of NFIA expression, speed, and efficiency did not match the results obtained with ectopic NFIA

expression, suggesting that further investigation into additional extrinsic factors is required to fully substitute for forced NFIA expression.

While it has become routine to model neurodevelopmental or neurodegenerative diseases[43,44] with hPSC-derived neurons, the use of hPSC-derived astrocytes in such studies has remained limited[7,45]. This is due in part, to the extremely protracted onset of the gliogenic switch in humans as compared to rodent cells, which is recapitulated *in vitro* and makes such studies laborious, costly, and inefficient. Our work presents a simple, effective strategy based on the use of a single factor to drive glial competency and astrocyte differentiation (Fig. 4N). Our ability to combine overexpression of *NFIA* with patterning of early stage NSCs enables the rapid derivation of region-specific astrocytes and will be of particular interest in studying the contribution of astrocytes to disorders affecting distinct brain regions, such as in Parkinson's disease, Alzheimer's disease, or ALS. Such region-specific astrocytes can be further harnessed for the study of distinct trophic support, as reported for primary astrocytes derived from discrete brain regions[46,47].

One potential concern in using *NFIA* to fast-forward human neural development is whether the resulting cell types match bona fide *in vivo*–derived astrocytes or represent an artifactual *in vitro* cell type. We demonstrate faithful transcriptional identity and robust functional features of NFIA-induced astrocytes, including calcium responses to relevant stimuli that not only match but exceed the performance of primary human fetal astrocytes. In addition, we show that NFIA-induced astrocytes reliably induce maturation of hPSC-derived neurons, a functional property commonly associated with mature, adult-like astrocytes[2]. Therefore, the NFIA-protocol yields astrocyte populations highly relevant for human molecular, physiological and disease-related studies.

Contrary to the role of NFIA overexpression in promoting competency for astrocyte differentiation, NFIA, when expressed at high levels, prevents further differentiation into astrocytes unless it is downregulated. We presume this is partially due to high levels of NFIA leading to G1 cell cycle arrest. It is possible that this finding explains the low efficiency of astrocyte induction in past ectopic expression studies in the chick spinal cord[13], and that *NFIA* levels need to be carefully titrated or followed by *NFIA* withdrawal to achieve optimal results. *NFIA* null mutant mice show a near complete loss of GFAP expression in the adult brain[48]. A similar phenotype is observed in Nuclear Factor 1B (*NFIB*) mutant mice[49]. The likely redundancy of *NFIA* and *NFIB in vivo* may explain why single mutant mice do not exhibit a more severe early developmental glial specification phenotype[3]. Further exploration of the interaction among TGFβ, NFIA/B and other factors in establishing the coordinated modulation of the cell cycle that promotes glial competency during *in vivo* development will be of particular interest. Another intriguing finding is that transient overexpression of *NFIA* is not sufficient to activate an irreversible, endogenous glial competency program in the absence of STAT or BMP signal activators. These results indicate that *NFIA* may act in concert with other factors such as *SOX9* to further stabilize the gliogenic program[50].

Our mechanistic studies demonstrate that *NFIA* can rapidly trigger a chromatin state similar to that of astrocytes. The gene expression data reveal that *NFIA* induces transcription of a

broad set of genes related to glial specification. Upon release of *NFIA* overexpression, several genes associated with astrocyte identity remain upregulated for at least 3 days, suggesting that *NFIA* may open the chromatin landscape at these particular genes to poise them for activation in response to extrinsic factors. We found the NFI- motif to be highly enriched in the accessible chromatin with *NFIA* expression. Other highly enriched motifs, such as the AP-1/JunB, require further study of their potential role in astrocyte differentiation or in maintenance of glial competency. The role of NFIA as a negative cell-cycle regulator was recapitulated in part by pharmacological or genetic modulation of the G1 phase. The role of the cell cycle in modulating cell fate decisions in undifferentiated hPSC populations has been described previously[51]. Our data demonstrate that NFIA expression lengthens G1, and that high NFIA levels trigger G1 arrest. Further exploration of the interaction among TGFβ, NFIA and other factors in establishing the coordinated, progressive modulation of the cell cycle that promotes the glial competent state during development will be of particular interest.

# METHODS

## Cell Culture

**Human pluripotent stem cells (hPSCs)—**(embryonic and induced) were maintained on Vitronectin coated dishes in Essential 8 (E8) media (Thermo) as previously described[52]. Induced pluripotent stem cells were purchased from Coriell, Patient normal lines 41865, 41866 and patient ALS (A4V) lines, 35659, 35673 and 35677. Cells were used for differentiation between passage 30–50 and passaged two times every week. Cells were subjected to mycoplasma testing every 2–3 months.

**Neural stem cells, LT-NSCs and glial progenitors—**were maintained on Poly-ornithine (PO), Laminin (Lam) and Fibronectin (FN) coated dishes in NSC media consisting of N2 media with 10ng/ml FGF2, 10ng/ml EGF and 1:1000 B27 supplement. LTNSCs were used between passage 15–20 and passaged every week.

**hPSC-derived astrocytes—**were maintained on PO/Lam/FN coated dishes in astrocyte media consisting of N2 media with 10ng/ml of HB-EGF (R&D Systems, 259-HE). After sorting, the CD44 positive cells were passaged every week for 4 weeks and then passaged every other week or until the astrocyte processes started to detach.

**Commercial fetal astrocytes—**(Sciencell) were initially maintained in a commercial media containing serum (Sciencell). The serum containing media was switched to N2 media with 10ng/ml of HB-EGF for at least 2 passages before experiments were performed.

**hPSC-derived cortical excitatory neurons—**were maintained on PO/Lam/FN coated dishes in Neurobasal media with BDNF, Ascorbic Acid, GDNF, Cyclic AMP (NB-BAGC). Greater than half of the media on the neurons were changed every week.

## Differentiation of hPSCs towards dorsal forebrain NSCs

**A. Dorsal forebrain patterning:** Human PSCs were dissociated into single cells and 2.5–3.0 $\times 10^5$ cells/cm$^2$ were plated onto Matrigel (BD Biosciences) coated dishes in E8 containing 10μM ROCK inhibitor (Y-27632). The next day (day 0), the cells were switched to Essential 6 (E6) media containing 100nM LDN193189 (LDN, Stemgent) and 10μM SB431542 (SB, Tocris) (LSB). The media was changed every day for 9 additional days (d8) as previously described[52]. To better promote an anterior forebrain fate (i.e. for iPSCs), one can add 2 μM of XAV939 (Stemgent) in addition to LSB for 3 days (d0-d2) then from d3-d8 maintain the cells in LSB without XAV.

**B. Generation of cortical rosettes/NSCs:** From d8, the cells are dissociated with Accutase for 30 minutes at 37ºC and passed through a 40-micron cell strainer. The cells resuspended in N2 media with BDNF, AA, SHH and FGF8 (N2-BASF) are then counted and plated on air-dried PO/Lam/FN plates as 2.5 × $10^4$ cells in 20μl droplets. The droplets are incubated at 37ºC for 15–20 minutes. N2-BASF8 + 10mM ROCKi media is overlaid on the droplets and media is changed every day. Rosette formation should be seen within 2–3 days after (d12).

After rosette formation, cells can be dissociated with Accutase and replated at relatively high density (3.5×$10^5$ cells/cm$^2$) to prevent spontaneous differentiation. Cultured cells can be assayed for correct regional patterning, differentiated or frozen.

## Neuroectodermal differentiation of hPSCs towards ventral spinal cord:

Similar to the dorsal forebrain, 2.5–3.0 $\times 10^5$ cells/cm$^2$ were plated onto Matrigel (BD Biosciences) coated dishes in hPSC KSR-based media containing 10μM ROCK inhibitor and 10 ng/ml FGF2. The next day (day 0), the cells were switched to a progressive gradient of KSR to N2 mediums containing 100nM LDN193189 and 10μM SB431542 (LSB). The next day (day 1), the media was switched to LSB with 1μM of retinoic acid and 1μM of purmorphamine and maintained in this media for an additional 11 days (d12).

Spinal cord progenitors are dissociated with Accutase for 30 minutes at 37ºC and passed through a 40-micron cell strainer. The cells are then replated at 2.5 × $10^5$ cells/cm$^2$ on PO/Lam/FN plates and assayed for correct regional patterning, differentiated or frozen.

## Derivation of LTNSCs from hPSCs

Initially, hPSCs are differentiated using the same method as the dorsal forebrain NSC. After the initial regional patterning, differentiated cells were dissociated using 10% Dispase for 10 minutes. Cells were then separated as clumps and resuspended in N2 media containing 20ng/ml FGF2 and cultured in sterile, non-TC treated dishes. Cells should form a high number of neurospheres and by 3–5 days neural rosette formation within the spheres should be apparent. Once the neurosphere cultures are pure, they are landed on PO/Lam/FN plates and cultured in N2 with 10ng/ml FGF2, 10ng/ml EGF and 1:1000 B27 supplement (NSC media). Rosette-stage NSC outgrowth is observed until confluency and then passaged at high density (roughly a 1:3 passage) over 2–3 months. Cells maintaining a neuroepithelial

morphology by passage 10 in NSC media were kept and analyzed for early NSC markers and differentiation potential.

### Generation of NFIA and SOX9 inducible constructs and lentiviral production and infection

NFIA and SOX9 were cloned from cDNA from hPSC-derived astroglial progenitors (d90). FUW-tetO-GFP (Addgene 30130) was digested with EcoRI to remove the GFP fragment and NFIA or SOX9 was inserted using traditional ligation cloning. Plasmids containing NFIA, SOX9, FUCCI-O or M2-rtTA (Addgene 20342), the psPAX2 (Addgene 12260) packaging vector and the pMD2.G (Addgene 12259) envelope was transfected into 293T cells using X-tremeGene HP (Sigma) in a 1:2:1 molar ratio, respectively. Virus was harvested at 48 and 72 hours post transfection and concentrated using AMICON Ultra-15 Centrifugal Filter Units (Millipore). NSCs were plated at $3.5\times10^5$ cells/$cm^2$ on PO/Lam/FN dishes. The cells were incubated with viral particles generated (described above) for 16–20 hours. The media is then switched to NSC media with 1–2μg/ml of doxycycline with daily media changes for a minimum of 5 days. Cells were then detached using 0.05% Trypsin and washed several times in preparation for CD44 labeling.

### Intracellular FACS analysis and sorting

For both live and fixed sorts, cells were dissociated using 0.05% Trypsin and washed 2 times with PBS.

**Fixed GFAP and CD44 analysis:** Using the BD Cytofix/Cytoperm kit (BD), $1\times10^6$ cells are resuspended in 1ml of Cytofix and placed on ice for 1 hour. The cells were then washed 2 times with 1X Cyto Perm Buffer and resuspended in 100μl of 1X Cyto Perm Buffer. Alexa 647 conjugated CD44 (Biolegend) and unconjugated GFAP (Dako) was added to the cells as described by the manufacturer and incubated for 40 minutes on ice. The cells were then washed 2 times with 1X Cyto Perm Buffer and resuspended in 100μl of 1X Cyto Perm Buffer for secondary labeling. Alexa 488 or 555 was added to the cells to label GFAP for 30 minutes on ice. Cells were washed 2 times with 1X Cyto Perm Buffer and taken for analysis.

**Live CD44 sort:** Approximately $4–5\times10^6$ cells were resuspended in 100μl of sort buffer (2% FBS, 1mM EDTA in PBS) and CD44 conjugated with Alexa 647 was incubated as per manufacturer's instructions on ice for 20–30 minutes. Cells were washed 2 times with sort buffer and taken to the sorter. CD44 positive cells were maintained in astrocyte induction media (N2 media with 10ng/ml HB-EGF (R&D Systems) and 10ng/ml Leukemia inhibitory factor (Peprotech) without doxycycline.

### Immunohistochemistry

Cells were fixed in PBS containing 4% paraformaldehyde (EMS) for 10 minutes and permeabilized using PBS with 0.5% Triton-X for 5 minutes and stored in PBS with 0.2% Tween-20. The blocking solution contained 5% donkey serum in PBS with 0.2% Tween-20. Primary antibodies were diluted in the blocking solution and typically incubated overnight at 4 C. Secondary antibodies conjugated to Alexa 488, Alexa 555 or Alexa 647 (Thermo) were added to the cells and incubated for 30 minutes. Nuclei were identified by staining the cells

with 4',6-diamidino-2-phenylindole (DAPI, Thermo). A list of antibodies used in this study is presented in Supplemental Table 3.

### Western blot

Cells were harvested, lysed with RIPA buffer and quantified using Precision Red. Ten micrograms of protein was loaded to analyze protein expression. Full scans of blots for Figure 2B (Supplemental Fig. 22), Figure 4F (Supplemental Fig. 23), Figure 4K (Supplemental Fig. 24) and Supplemental Figure 7C (Supplemental Figure 25) are available.

### Gene expression and ATAC-Seq analysis

**RNA-sequencing:** RNA was isolated as previously described. Total RNA was submitted to the MSKCC Genomics Core for paired-end sequencing aiming for 30–40 million reads. Raw FASTQ files were trimmed for adapters and aligned to the ENSEMBL GRCh38 genome build using STAR 2.5.0. Matrices were generated from the aligned files using HTSeq[53] and imported into DESeq2[54] for further analysis using a standard pipeline. A table for the normalized read counts represented in Figure 1 and Supplemental Fig. 8 can be found in Supplemental Table 1 and list of genes expressed from each sample in Figure 4 can be found in Supplemental Table 2.

**ATAC-sequencing:** Raw FASTQ files were aligned to the hg19 genome build using Bowtie2[55]. Comparative analysis of alignment files was performed using the deepTools software package[56]. Motif analysis and peak annotation was performed using the HOMER software[57] and visualized using the IGV browser[58].

All FASTQ files and supplemental files are uploaded to NCBI GEO under the accession GSE104232.

### Cytokine treatment of human astrocytes

Astrocytes were plated at $2\times10^4$ cells/cm$^2$ and treated with 3 ng/ml IL-1α (Sigma), 30ng/ml TNF (Cell Signaling Tech) and 400 ng/ml C1q (MyBioSource) for 24 hours. The media was isolated and spun down to remove debris and the levels of C3 were measured using the Human Complement C3 ELISA Kit (Abcam) as per manufacturer's instructions.

### Cell Cycle Analysis

Cells were dissociated nuclei were isolated using a resuspension buffer (10mM Tris-HCl, 30mM NaCl, 20mM MgCl2) and subsequently the resuspension buffer with 1% NP-40 for cell cycle analysis. Propidium Iodine (250ng/ml) was added to the cells and analyzed by FACS. A minimum of 10,000 events was analyzed per condition. Data acquired was imported and analyzed by the Flowjo software.

### Transplantation of NSCs, glial precursors and astrocytes into adult cortex

All surgeries were performed according to the NIH guidelines, and were approved by the local Institutional Animal Care and Use Committee (IACUC), the Institutional Biosafety Committee (IBC) and the Embryonic Stem Cell Research Committee (ESCRO). A total of 8 (or 20) [CF1] NOD-SCID IL2-Rgc null mice (20–35 g; Jackson Laboratory) received cell

transplantation. Mice were anesthetized with isoflurane 5% and kipping maintenance flow of 2–3%. A total of $7\times10^4$ NFIA-induced astrocytes in 2μl were transplanted through a 5μl-Hamilton syringe at a rate of 1μl/min by an infusion pump attached to a stereotactic micromanipulator, into the genu of the corpus callosum (coordinates: AP +0.740, ML −1.00, DV −2.30 from bregma). A total of $2\times10^5$ LTNSCs/2μl were transplanted into the subcortical gray matter, striatum (coordinates AP +0.500, ML −1.900, DV −3.200 from bregma). A total of $7.5\times10^4$ H1 derived-Astrocytes GFP- in 2μl was transplanted into the genu of the corpus callosum (coordinates: AP+0.740, ML −1.00, DV-2.30 from bregma). The mice were sacrificed at 1, 6 and 12 weeks after transplantation for IHC analysis.

## Tissue processing

Mice were euthanized with overdose of pentobarbital intraperitoneally and transcardially perfused with phosphate buffered saline then paraformaldehyde (PFA) 4%. Brains were removed after gentle dissection and kept in overnight 4% PFA then soaked in 30% sucrose for 2–3 days. Brain coronal sections of 30μm thick at −20°C were performed by cryostat after embedding the brain with O.C.T (Sakura Finetek).

## Calcium Imaging

hPSC-derived neural stem cells or astrocytes and primary astrocytes (Sciencell) were plated onto PO/Laminin/Fibronectin coated 0.5mm black ΔT dishes (Bioptechs) and used for calcium imaging as previously described[59] between days 60 and 120 from hPSCs. Cultures were incubated with 5uM of Fura-2 (Thermo) for 30 minutes at 37 C and dishes were mounted to a ΔT Heated Lid w/ Perfusion system (Bioptechs). Cultures were perfused with normal Tyrode's solution (pH 7.4) containing 125mM NaCl, 5mM KCl, 25mM Glucose, 25mM HEPES, 1mM $MgCl_2$, 2mM $CaCl_2$ and 0.1% (w/v) bovine serum albumin. Cultures were supplemented with glutamate (100$\mu$M), ATP (30$\mu$M) or KCl (65mM) for 1 minute and imaged every 30 seconds at 340 and 380 nm at a minimum of 7 positions. Time-lapse images were analyzed using FIJI (ImageJ) by calculating the signal ratio between 380/340 nm.

## Glutamate Excitotoxicity assay

Cortical neurons were derived by differentiating hPSCs towards the neuroectodermal fate (see above). Neuroectodermal cells were then dissociated and replated to generate neural rosettes and further differentiated into neurons by the treatment with DAPT. Neurons were then replated and assayed for maturation markers or glutamate excitoxicity[60] with or without astrocytes. For glutamate excitotoxicity studies, 100,000 neurons/$cm^2$ were plated on PO/Laminin/Fibronectin dishes in N2 media with BDNF, AA, and GDNF. NFIA-induced astrocytes were added at 150,000 cells/$cm^2$ and co-cultured for an additional 5 days. Cells were then treated with 100 or 500 μm (final) of L-glutamate for 1 hour in HBSS and recovered in N2 media with BDNF, AA, and GDNF. Resazurin was added 48 hours after glutamate treatment to determine cell viability.

### Bisulfite conversion and sequencing

LTNSCs infected with NFIA were treated with dox for 5 days and sorted for CD44. Cells were isolated and bisulfite conversion was performed using the EZ DNA Methylation-Direct™ Kit (Zymo) as described by manufacturer. Primers to the regions of the GFAP STAT3 binding site was described previously[61]. Briefly, P1 and P2 corresponds to −1500bp from the start site of GFAP (P1 forward: 5' AGGAGGGTTGTTTGTTTTTTAGAA, P1 reverse: 5' CCCTTCCTTATCTAACCTCCCTATA and P2 forward = 5' GTAGATTTGGTAGTATTGGGTTGGT, P2 reverse = 5' CCCTCACCCATTTATATCCTTAAA. The GFAP promoter region was amplified using ZymoTaq Premix (Zymo) and cloned into the TOPO Zero Blunt vector (Invitrogen). A minimum of 10 colonies were sent for sequencing per condition.

### Electrophysiology

Whole-cell recordings were performed as described previously[62], with slight modifications. Briefly, neurons were visualized using a Zeiss microscope (Axioscope) equipped with a 4x objective and a 40x water immersion. Neurons were recorded at 23 – 24 °C. Input resistance was measured from a voltage response elicited by intracellular injection of a current pulse (−100 pA, 200 ms). Membrane voltage was low-pass filtered at 5 kHz and digitized at 10 kHz using, a Multiclamp 700B amplifier connected to a DigiData 1322A interface (Axon Instruments) using Clampex 10.2 software (Molecular Devices, Foster City, CA). Liquid junction potentials were calculated and corrected off-line[63]. During recordings, neurons were perfused with freshly prepared ACSF which contained (in mM): 126 NaCl, 26 NaHCO3, 3.6 KCl, 1.2 NaH2PO4, 1.5MgCl2, 2.5 CaCl2, and 10 glucose, and the solution was saturated with 95% O2 – 5% CO2. Pipette solution for all recordings contained (in mM): 140 CsCl, 10 NaCl, 10 HEPES, 0.5 EGTA, 3 Mg-ATP, 0.2 Na-GTP, and 10 Na2-phosphocreatine, pH adjusted to 7.3 with CsOH. 20μM (−)-Bicuculline methochloride (Tocris), 1 μM strychnine HCl (Sigma) and 0.5 μM tetrodotoxin (TTX) (Alomone Labs) were added to the ACSF for mEPSC recordings to block GABA receptors, glycine receptors and Na+ channels respectively. Neurons were held at −80mV and continuous recordings of mEPSCs were made using Axoscope software (Molecular Devices, Union City, CA). Data processing and analysis were performed using MiniAnalysis (Synaptosoft, Decatur, GA) and Clampfit 10 (Molecular Devices). Events were detected by setting the threshold value, followed by visual confirmation of mEPSC detection. Statistical analysis was performed using Student's t test or Mann-Whitney Rank Sum test as necessary, with a significant difference at $P < 0.05$. Data are expressed as mean ± SE.

### DATA AVAILABILITY

The data and reagents in this study are available from the corresponding author upon reasonable request.

## Supplementary Material

Refer to Web version on PubMed Central for supplementary material.

## ACKNOWLEDGEMENTS

We are grateful to the members the Studer lab for helpful discussions and support for this project and G. Cederquist, M. Tomishima, S. Irion and V. Tabar for their critical comments on the manuscript. We would also like to especially thank A. Koff (MSKCC) for his helpful comments, experimental discussions regarding the cell cycle and comments on the manuscript. Additionally, we would like to thank A. Viale at Integrated Genomics Operation Core (MSKCC) for the RNA-sequencing studies, M. Witkin at the Epigenetics Core (MSKCC) for the ATAC-sequencing, S. Fujisawa, E. Feng and V.Boyko at the Molecular Cytology Core (MSKCC) for help in calcium imaging studies and quantification of synaptic proteins, R. Garripa and H. Liu at the RNAi Core (MSKCC) for help in shRNA design and the Flow Cytometry Core (MSKCC) for the cell sorting applications. J.T. was supported by the Tri-I Starr Stem Cell Scholars postdoctoral training fellowship. S.R.G was supported by the Ruth L. Kirschstein Individual Predoctoral NRSA for MD/PhD Fellowship (1F30MH115616–01) and by a Medical Scientist Training Program grant from the National Institute of General Medical Sciences of the National Institutes of Health under award number

(T32GM007739) to the Weill Cornell/Rockefeller/Sloan Kettering Tri-Institutional MD -PhD Program. E.M.G. was supported by a grant from the Schweizerischer Nationalfonds zur Förderung der Wissenschaftlichen Forschung (323630–164217). The work was supported by grants from the National Institutes of Health R21NS084334 (LS) and the core grant P30CA008748.

## References

1. Liddelow SA et al. Neurotoxic reactive astrocytes are induced by activated microglia. Nature 541, 481–487, doi:10.1038/nature21029 (2017). [PubMed: 28099414]
2. Zhang Y et al. Purification and Characterization of Progenitor and Mature Human Astrocytes Reveals Transcriptional and Functional Differences with Mouse. Neuron 89, 37–53, doi:10.1016/j.neuron.2015.11.013 (2016). [PubMed: 26687838]
3. Molofsky AV et al. Astrocytes and disease: a neurodevelopmental perspective. Genes Dev 26, 891–907, doi:10.1101/gad.188326.112 (2012). [PubMed: 22549954]
4. Sauvageot CM & Stiles CD Molecular mechanisms controlling cortical gliogenesis. Current opinion in neurobiology 12, 244–249 (2002). [PubMed: 12049929]
5. Studer L, Vera E & Cornacchia D Programming and Reprogramming Cellular Age in the Era of Induced Pluripotency. Cell Stem Cell 16, 591–600, doi:10.1016/j.stem.2015.05.004 (2015). [PubMed: 26046759]
6. Tcw J et al. An Efficient Platform for Astrocyte Differentiation from Human Induced Pluripotent Stem Cells. Stem Cell Reports 9, 600–614, doi:10.1016/j.stemcr.2017.06.018 (2017). [PubMed: 28757165]
7. Krencik R et al. Dysregulation of astrocyte extracellular signaling in Costello syndrome. Sci Transl Med 7, 286ra266, doi:10.1126/scitranslmed.aaa5645 (2015).
8. Tao Y & Zhang SC Neural Subtype Specification from Human Pluripotent Stem Cells. Cell Stem Cell 19, 573–586, doi:10.1016/j.stem.2016.10.015 (2016). [PubMed: 27814479]
9. Chandrasekaran A, Avci HX, Leist M, Kobolak J & Dinnyes A Astrocyte Differentiation of Human Pluripotent Stem Cells: New Tools for Neurological Disorder Research. Front Cell Neurosci 10, 215, doi:10.3389/fncel.2016.00215 (2016). [PubMed: 27725795]
10. Santos R et al. Differentiation of Inflammation-Responsive Astrocytes from Glial Progenitors Generated from Human Induced Pluripotent Stem Cells. Stem Cell Reports 8, 1757–1769, doi:10.1016/j.stemcr.2017.05.011 (2017). [PubMed: 28591655]
11. Krencik R, Weick JP, Liu Y, Zhang ZJ & Zhang SC Specification of transplantable astroglial subtypes from human pluripotent stem cells. Nat Biotechnol 29, 528–534, doi:10.1038/nbt.1877 (2011). [PubMed: 21602806]
12. Stolt CC et al. The Sox9 transcription factor determines glial fate choice in the developing spinal cord. Genes Dev 17, 1677–1689, doi:10.1101/gad.259003 (2003). [PubMed: 12842915]
13. Deneen B et al. The transcription factor NFIA controls the onset of gliogenesis in the developing spinal cord. Neuron 52, 953–968, doi:10.1016/j.neuron.2006.11.019 (2006). [PubMed: 17178400]
14. Patterson M et al. let-7 miRNAs can act through notch to regulate human gliogenesis. Stem Cell Reports 3, 758–773, doi:10.1016/j.stemcr.2014.08.015 (2014). [PubMed: 25316189]

15. Naka H, Nakamura S, Shimazaki T & Okano H Requirement for COUP-TFI and II in the temporal specification of neural stem cells in CNS development. Nat Neurosci 11, 1014–1023, doi: 10.1038/nn.2168 (2008). [PubMed: 19160499]
16. Hirabayashi Y et al. Polycomb limits the neurogenic competence of neural precursor cells to promote astrogenic fate transition. Neuron 63, 600–613, doi:10.1016/j.neuron.2009.08.021 (2009). [PubMed: 19755104]
17. Koch P, Opitz T, Steinbeck JA, Ladewig J & Brustle O A rosette-type, self-renewing human ES cell-derived neural stem cell with potential for in vitro instruction and synaptic integration. Proc Natl Acad Sci U S A 106, 3225–3230, doi:10.1073/pnas.0808387106 (2009). [PubMed: 19218428]
18. Elkabetz Y et al. Human ES cell-derived neural rosettes reveal a functionally distinct early neural stem cell stage. Genes Dev 22, 152–165, doi:10.1101/gad.1616208 (2008). [PubMed: 18198334]
19. Liu Y et al. CD44 expression identifies astrocyte-restricted precursor cells. Dev Biol 276, 31–46, doi:10.1016/j.ydbio.2004.08.018 (2004). [PubMed: 15531362]
20. Chen H et al. Modeling ALS with iPSCs reveals that mutant SOD1 misregulates neurofilament balance in motor neurons. Cell Stem Cell 14, 796–809, doi:10.1016/j.stem.2014.02.004 (2014). [PubMed: 24704493]
21. Calder EL et al. Retinoic Acid-Mediated Regulation of GLI3 Enables Efficient Motoneuron Derivation from Human ESCs in the Absence of Extrinsic SHH Activation. J Neurosci 35, 11462–11481, doi:10.1523/JNEUROSCI.3046-14.2015 (2015). [PubMed: 26290227]
22. Magistri M et al. A comparative transcriptomic analysis of astrocytes differentiation from human neural progenitor cells. Eur J Neurosci 44, 2858–2870, doi:10.1111/ejn.13382 (2016). [PubMed: 27564458]
23. Lovatt D et al. The transcriptome and metabolic gene signature of protoplasmic astrocytes in the adult murine cortex. J Neurosci 27, 12255–12266, doi:10.1523/JNEUROSCI.3404-07.2007 (2007). [PubMed: 17989291]
24. Cahoy JD et al. A transcriptome database for astrocytes, neurons, and oligodendrocytes: a new resource for understanding brain development and function. J Neurosci 28, 264–278, doi:10.1523/JNEUROSCI.4178-07.2008 (2008). [PubMed: 18171944]
25. Doyle JP et al. Application of a translational profiling approach for the comparative analysis of CNS cell types. Cell 135, 749–762, doi:10.1016/j.cell.2008.10.029 (2008). [PubMed: 19013282]
26. Ullian EM, Sapperstein SK, Christopherson KS & Barres BA Control of synapse number by glia. Science 291, 657–661, doi:10.1126/science.291.5504.657 (2001). [PubMed: 11158678]
27. Sofroniew MV Astrocyte barriers to neurotoxic inflammation. Nat Rev Neurosci 16, 249–263, doi: 10.1038/nrn3898 (2015). [PubMed: 25891508]
28. Allen NJ & Eroglu C Cell Biology of Astrocyte-Synapse Interactions. Neuron 96, 697–708, doi: 10.1016/j.neuron.2017.09.056 (2017). [PubMed: 29096081]
29. Betz A et al. Munc13–1 is a presynaptic phorbol ester receptor that enhances neurotransmitter release. Neuron 21, 123–136 (1998). [PubMed: 9697857]
30. Sofroniew MV & Vinters HV Astrocytes: biology and pathology. Acta Neuropathol 119, 7–35, doi: 10.1007/s00401-009-0619-8 (2010). [PubMed: 20012068]
31. Liddelow SA & Barres BA Reactive Astrocytes: Production, Function, and Therapeutic Potential. Immunity 46, 957–967, doi:10.1016/j.immuni.2017.06.006 (2017). [PubMed: 28636962]
32. Cornell-Bell AH, Finkbeiner SM, Cooper MS & Smith SJ Glutamate induces calcium waves in cultured astrocytes: long-range glial signaling. Science 247, 470–473 (1990). [PubMed: 1967852]
33. Oberheim NA et al. Uniquely hominid features of adult human astrocytes. J Neurosci 29, 3276–3287, doi:10.1523/JNEUROSCI.4707-08.2009 (2009). [PubMed: 19279265]
34. Rajan P & McKay RD Multiple routes to astrocytic differentiation in the CNS. J Neurosci 18, 3620–3629 (1998). [PubMed: 9570793]
35. Huang da W, Sherman BT & Lempicki RA Systematic and integrative analysis of large gene lists using DAVID bioinformatics resources. Nat Protoc 4, 44–57, doi:10.1038/nprot.2008.211 (2009). [PubMed: 19131956]

36. Takahashi T, Nowakowski RS & Caviness VS Jr. The cell cycle of the pseudostratified ventricular epithelium of the embryonic murine cerebral wall. J Neurosci 15, 6046–6057 (1995). [PubMed: 7666188]
37. Sakaue-Sawano A et al. Visualizing spatiotemporal dynamics of multicellular cell-cycle progression. Cell 132, 487–498, doi:10.1016/j.cell.2007.12.033 (2008). [PubMed: 18267078]
38. Calegari F & Huttner WB An inhibition of cyclin-dependent kinases that lengthens, but does not arrest, neuroepithelial cell cycle induces premature neurogenesis. J Cell Sci 116, 4947–4955, doi: 10.1242/jcs.00825 (2003). [PubMed: 14625388]
39. Vodermaier HC APC/C and SCF: controlling each other and the cell cycle. Curr Biol 14, R787–796, doi:10.1016/j.cub.2004.09.020 (2004). [PubMed: 15380093]
40. Sigl R et al. Loss of the mammalian APC/C activator FZR1 shortens G1 and lengthens S phase but has little effect on exit from mitosis. J Cell Sci 122, 4208–4217, doi:10.1242/jcs.054197 (2009). [PubMed: 19861496]
41. Garcia-Campmany L & Marti E The TGFbeta intracellular effector Smad3 regulates neuronal differentiation and cell fate specification in the developing spinal cord. Development 134, 65–75, doi:10.1242/dev.02702 (2007). [PubMed: 17138664]
42. Zhang Y, Alexander PB & Wang XF TGF-beta Family Signaling in the Control of Cell Proliferation and Survival. Cold Spring Harb Perspect Biol 9, doi:10.1101/cshperspect.a022145 (2017).
43. Zeltner N & Studer L Pluripotent stem cell-based disease modeling: current hurdles and future promise. Curr Opin Cell Biol 37, 102–110, doi:10.1016/j.ceb.2015.10.008 (2015). [PubMed: 26629748]
44. Sances S et al. Modeling ALS with motor neurons derived from human induced pluripotent stem cells. Nat Neurosci 19, 542–553, doi:10.1038/nn.4273 (2016). [PubMed: 27021939]
45. Williams EC et al. Mutant astrocytes differentiated from Rett syndrome patients-specific iPSCs have adverse effects on wild-type neurons. Hum Mol Genet 23, 2968–2980, doi:10.1093/hmg/ddu008 (2014). [PubMed: 24419315]
46. Le Roux PD & Reh TA Astroglia demonstrate regional differences in their ability to maintain primary dendritic outgrowth from mouse cortical neurons in vitro. J Neurobiol 27, 97–112, doi: 10.1002/neu.480270110 (1995). [PubMed: 7643079]
47. Holmqvist S et al. Generation of human pluripotent stem cell reporter lines for the isolation of and reporting on astrocytes generated from ventral midbrain and ventral spinal cord neural progenitors. Stem Cell Res 15, 203–220, doi:10.1016/j.scr.2015.05.014 (2015). [PubMed: 26100233]
48. das Neves L et al. Disruption of the murine nuclear factor I-A gene (Nfia) results in perinatal lethality, hydrocephalus, and agenesis of the corpus callosum. Proc Natl Acad Sci U S A 96, 11946–11951 (1999). [PubMed: 10518556]
49. Steele-Perkins G et al. The transcription factor gene Nfib is essential for both lung maturation and brain development. Molecular and cellular biology 25, 685–698, doi:10.1128/MCB.25.2.685-698.2005 (2005). [PubMed: 15632069]
50. Canals I et al. Rapid and efficient induction of functional astrocytes from human pluripotent stem cells. Nat Methods 15, 693–696, doi:10.1038/s41592-018-0103-2 (2018). [PubMed: 30127505]
51. Pauklin S & Vallier L The cell-cycle state of stem cells determines cell fate propensity. Cell 155, 135–147, doi:10.1016/j.cell.2013.08.031 (2013). [PubMed: 24074866]
52. Tchieu J et al. A Modular Platform for Differentiation of Human PSCs into All Major Ectodermal Lineages. Cell Stem Cell 21, 399–410 e397, doi:10.1016/j.stem.2017.08.015 (2017). [PubMed: 28886367]
53. Anders S, Pyl PT & Huber W HTSeq--a Python framework to work with high-throughput sequencing data. Bioinformatics 31, 166–169, doi:10.1093/bioinformatics/btu638 (2015). [PubMed: 25260700]
54. Love MI, Huber W & Anders S Moderated estimation of fold change and dispersion for RNA-seq data with DESeq2. Genome Biol 15, 550, doi:10.1186/s13059-014-0550-8 (2014). [PubMed: 25516281]
55. Langmead B & Salzberg SL Fast gapped-read alignment with Bowtie 2. Nature methods 9, 357–359, doi:10.1038/nmeth.1923 (2012). [PubMed: 22388286]

56. Ramirez F et al. deepTools2: a next generation web server for deep-sequencing data analysis. Nucleic Acids Res 44, W160–165, doi:10.1093/nar/gkw257 (2016). [PubMed: 27079975]
57. Heinz S et al. Simple combinations of lineage-determining transcription factors prime cis-regulatory elements required for macrophage and B cell identities. Mol Cell 38, 576–589, doi: 10.1016/j.molcel.2010.05.004 (2010). [PubMed: 20513432]
58. Robinson JT et al. Integrative genomics viewer. Nat Biotechnol 29, 24–26, doi:10.1038/nbt.1754 (2011). [PubMed: 21221095]
59. Steinbeck JA et al. Functional Connectivity under Optogenetic Control Allows Modeling of Human Neuromuscular Disease. Cell Stem Cell 18, 134–143, doi:10.1016/j.stem.2015.10.002 (2016). [PubMed: 26549107]
60. Chiricozzi E et al. Group IIA secretory phospholipase A2 (GIIA) mediates apoptotic death during NMDA receptor activation in rat primary cortical neurons. J Neurochem 112, 1574–1583, doi: 10.1111/j.1471-4159.2010.06567.x (2010). [PubMed: 20067579]
61. Cheng PY et al. Interplay between SIN3A and STAT3 mediates chromatin conformational changes and GFAP expression during cellular differentiation. PLoS One 6, e22018, doi:10.1371/journal.pone.0022018 (2011). [PubMed: 21779366]
62. Maroof AM et al. Directed differentiation and functional maturation of cortical interneurons from human embryonic stem cells. Cell Stem Cell 12, 559–572, doi:10.1016/j.stem.2013.04.008 (2013). [PubMed: 23642365]
63. Ying SW & Goldstein PA Propofol suppresses synaptic responsiveness of somatosensory relay neurons to excitatory input by potentiating GABA(A) receptor chloride channels. Mol Pain 1, 2, doi:10.1186/1744-8069-1-2 (2005). [PubMed: 15813991]

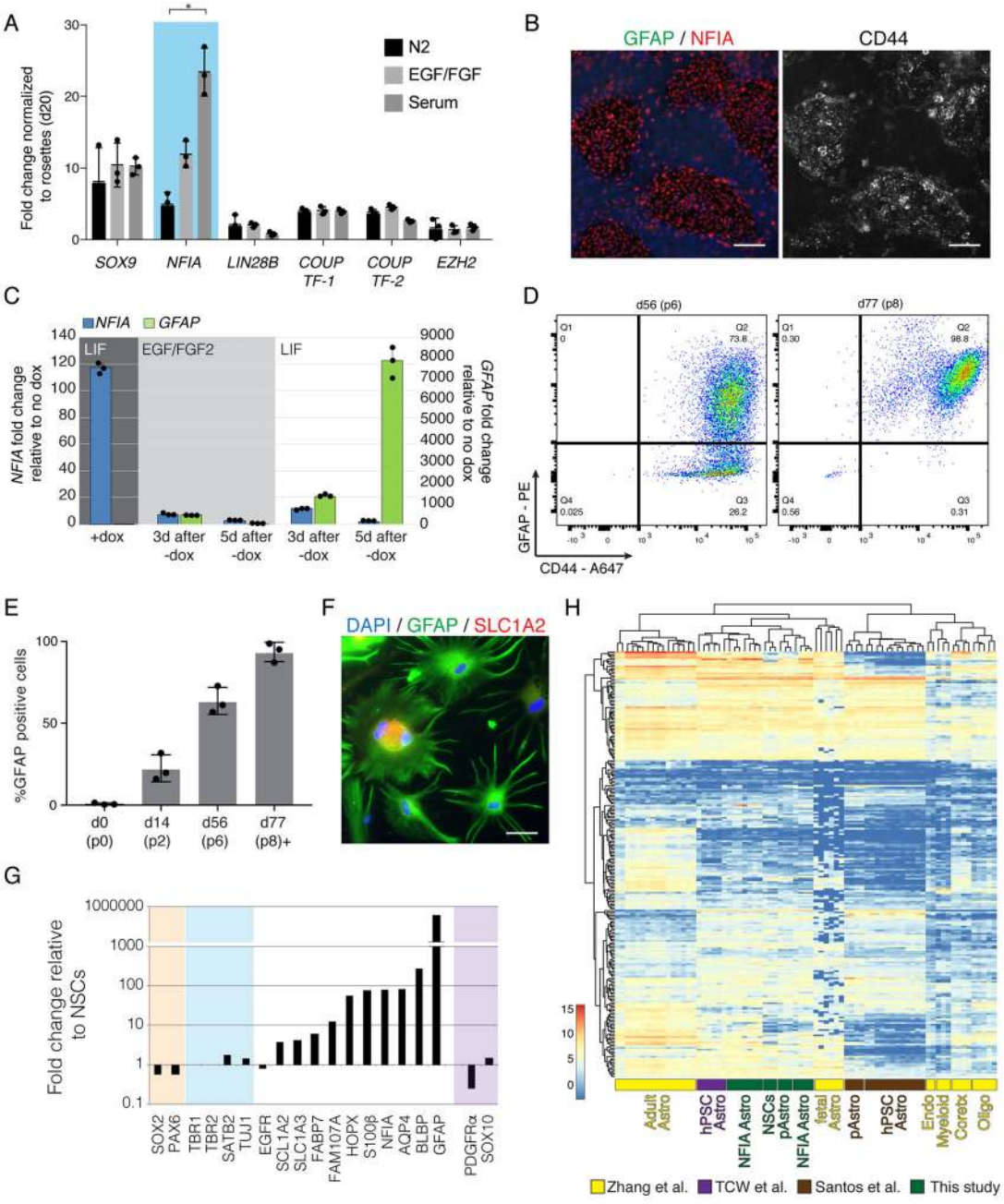


**Fig. 1. Transient expression of NFIA in neuroepithelial stem cells confers glial competency.**

**A**, Quantitative PCR of candidate genes associated with glial competency treated in serum (1% FBS) conditions for 30 days. **One-way ANOVA (p-value = 0.025, n= 3 biologically independent experiments, mean values are represented by a black bar). **B**, Overexpression of NFIA leads to profound morphological changes within 5 days of doxycycline treatment marked by yellow arrowheads (n= 5 biologically independent experiments). **C**, Quantitative PCR analysis of GFAP and NFIA expression in NSCs treated with doxycycline for 5 days and subsequent removal for an additional 3 and 5 days or continuous treatment (+dox) (n= 3 biologically independent experiments, mean values are represented in bar graph). **D**,

Intracellular FACS analysis for GFAP and CD44 during the differentiation of NFIA-induced NSCs at 56 (p6) and 77 (p8). **E**, Quantification of the percentage of GFAP expressing cells at different timepoints (n=3 biologically independent experiments, mean values are represented in bar graph). **F**, Immunofluorescence staining of GFAP and SLC1A2 in d60 astrocyte culture (n= 5 biologically independent experiments). **G**, Quantitative PCR analysis of genes associated with NSCs, neurons, astrocytes and oligodendrocytes from NFIA-induced astrocytes. **H**, Heatmap of normalized read-counts representing genes associated with astrocyte identity (Supplemental Table 1). Yellow = Zhang et al., purple = TCW et al., brown = Santos et al., green = this study. Scale bars are 50 $\mu$m. Error bars are calculated by S.E.M.

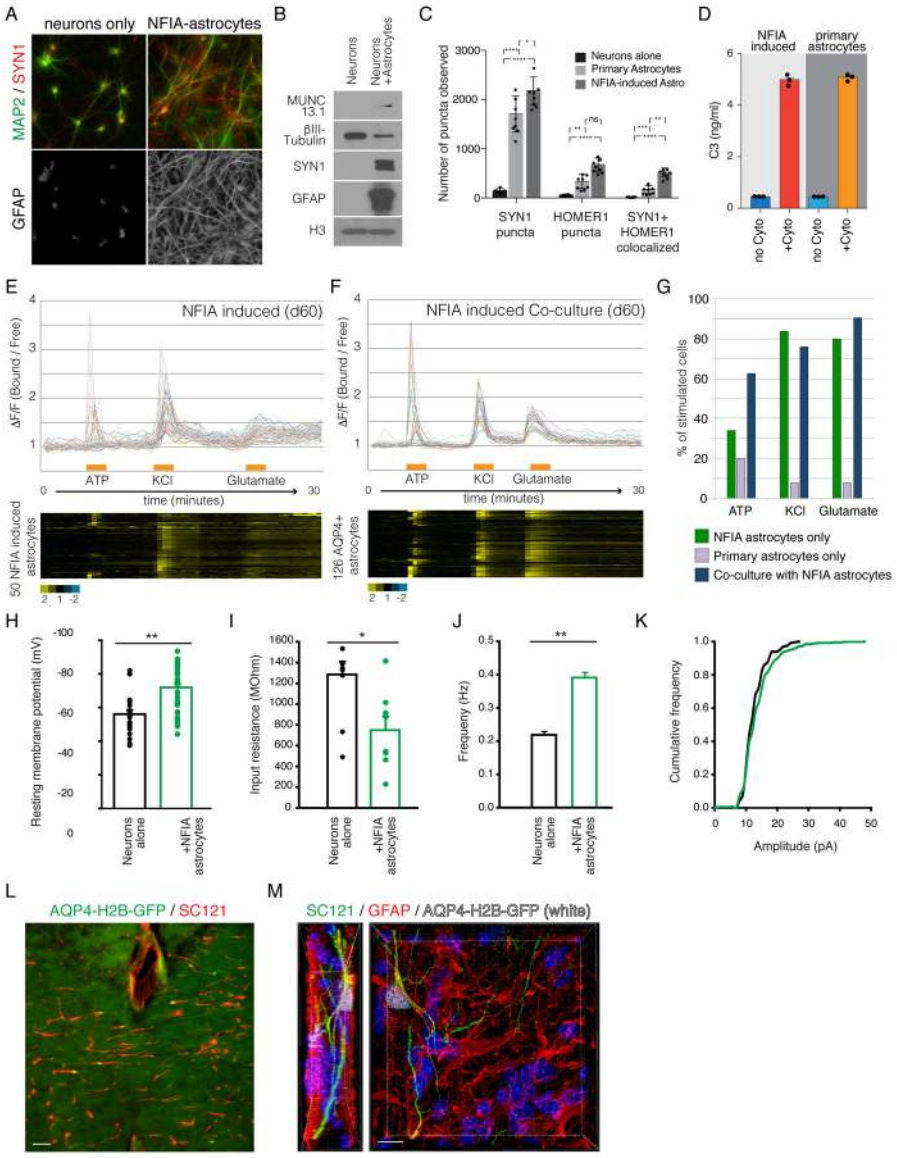


**Fig. 2. NFIA-induced astrocytes are functional.**

**A**, Immunofluorescence staining of MAP2 and synapsin-1 (SYN1) on neurons cultured with or without NFIA-induced astrocytes (n= 3 biologically independent experiments). **B**, Western blot analysis of markers of maturity, MUNC13.1 and SYN1 in neurons cultured with or without astrocytes (n= 3 biologically independent experiments). **C**, A bar chart representing the quantification of SYN1 and HOMER1 puncta on TUJ1 positive neurons (n=8 biologically independent experiments, mean values are represented in the bar graph) cultured with or without astrocytes for 28 days. One-way ANOVA *(p-value < 0.05), **(p-value < 0.01), ****(p-value < 0.001). **D**, Bar chart representing the amount of complement (C3) released from NFIA-induced or primary astrocytes treated with IL1α, TNF and C1q for 24 hours (n=3 biologically independent experiments, mean values are presented in bar graph). **E**, Ratiometric plots of purified NFIA-induced astrocytes (60 days) incubated with the Fura-2 calcium dye and stimulated with ATP, KCl and Glutamate. All data points are

plotted as a heatmap below. **F**, Ratiometric plots of NFIA-induced astrocytes co-cultured with neurons incubated with the Fura-2 calcium dye and stimulated with ATP, KCl and Glutamate. Ratios were calculated on GFP positive nuclei. All data points are plotted as a heatmap below. **G**, Quantification of the number of astrocytes responding to ATP, KCl or Glutamate from data presented in E, F and Supplemental Data Fig. 13. H, Quantification of the resting membrane potential. Student's t-test p-value = 0.0000186, n=23, 39. **I**, Quantification of the mean input resistance. Student's t-test p-value = 0.010, n=10, 8. **J**, Mean frequency of neurons with or without astrocytes. Mann-Whitney Rank Sum p-value = 0.000155. **K**, Cumulative distribution of all the mEPSC amplitudes recorded. For control neurons 341 mEPSCs were recorded from 10 neurons and for neurons in the presence of glia 629 mEPSCs were recorded from 6 neurons. All electrophysiology was performed on 3 biologically independent experiments. **L**, Immunofluorescence of NFIA-induced glial progenitors transplanted into the mouse cortex depict migration through the corpus callosum (n=3 biologically independent animals). Scale bar 50 μm. **M**, Immunofluorescence of NFIA-induced astrocytes demonstrate co-expression of AQP4-H2B-GFP, GFAP and the human specific marker SC-121 (n=3 biologically independent animals). Scale bar 10 μm.

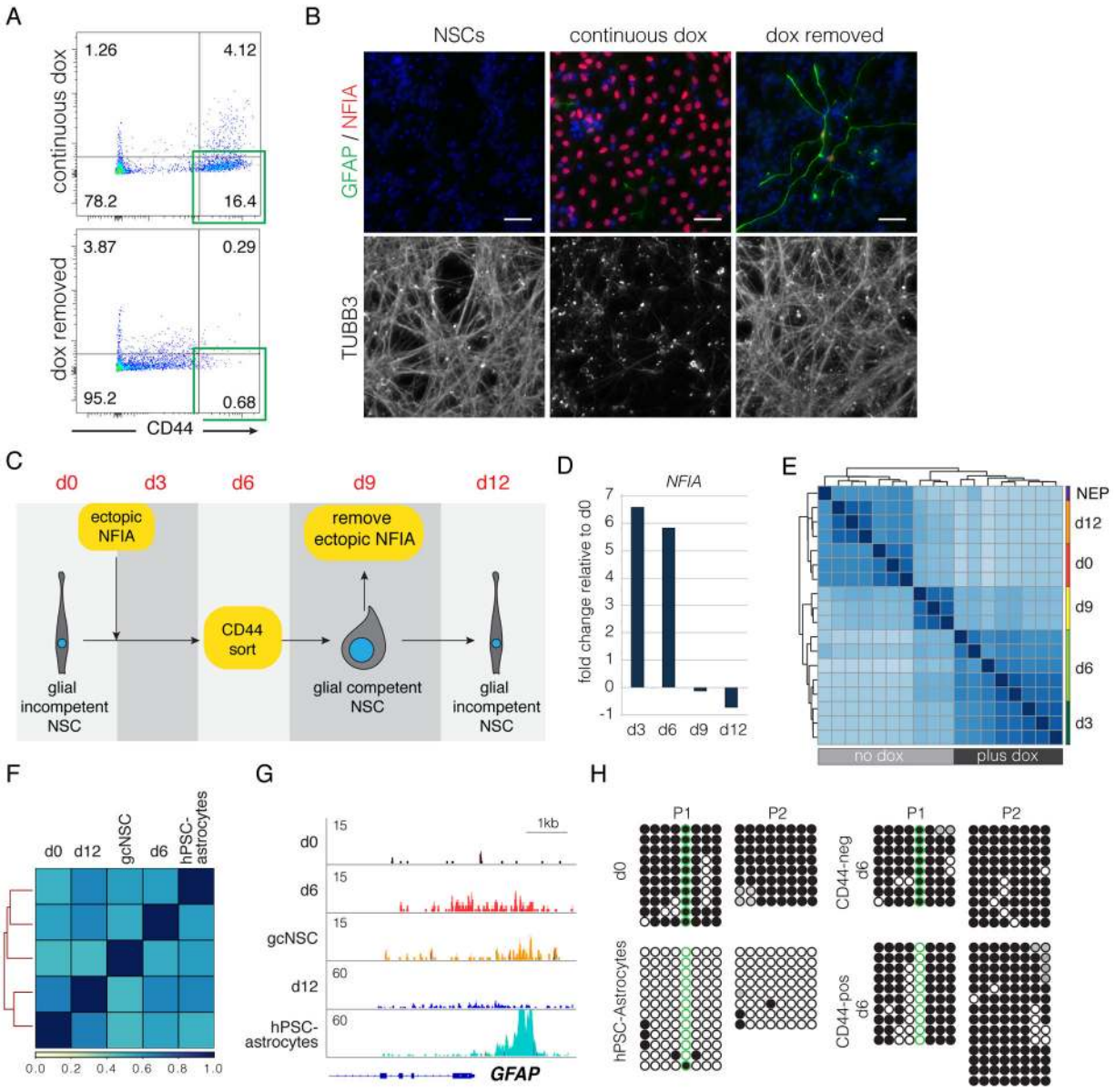


**Fig. 3. NFIA cannot maintain the glial competent state.**

**A**, FACS plot of CD44 expressing cells treated with continuous doxycycline or doxycycline removed demonstrates that CD44 expression is lost after doxycycline removal. **B**, Immunofluorescence staining for NFIA, GFAP and TUBB3 in NSCs, NFIA-induced NSCs and NFIA-induced NSCs with doxycycline removal (n= 3 biologically independent experiments). **C**, Schematic representation of cells induced with NFIA and attaining glial competency then reversal to glial incompetency with doxycycline withdrawal. **D**, Quantitative PCR data of NFIA expression along the time course represented in C. **E**, Sample distance plot for RNA expression of NSCs at different timepoints related C. **F**, Sample distance plot for chromatin accessibility compared to glial competent NSCs (gcNSCs) and hPSC-derived astrocytes (200 days of in vitro culture). **G**, Example ATAC-seq tracks at the GFAP locus that depicts the lack of chromatin accessibility in several NSC

samples. **H**, Bisulfite sequencing of the promoter region of the GFAP promoter (P1 and P2) suggests that CD44 positive cells resulting from overexpression of NFIA leads to demethylation of a specific CpG on the GFAP promoter (circled in green).

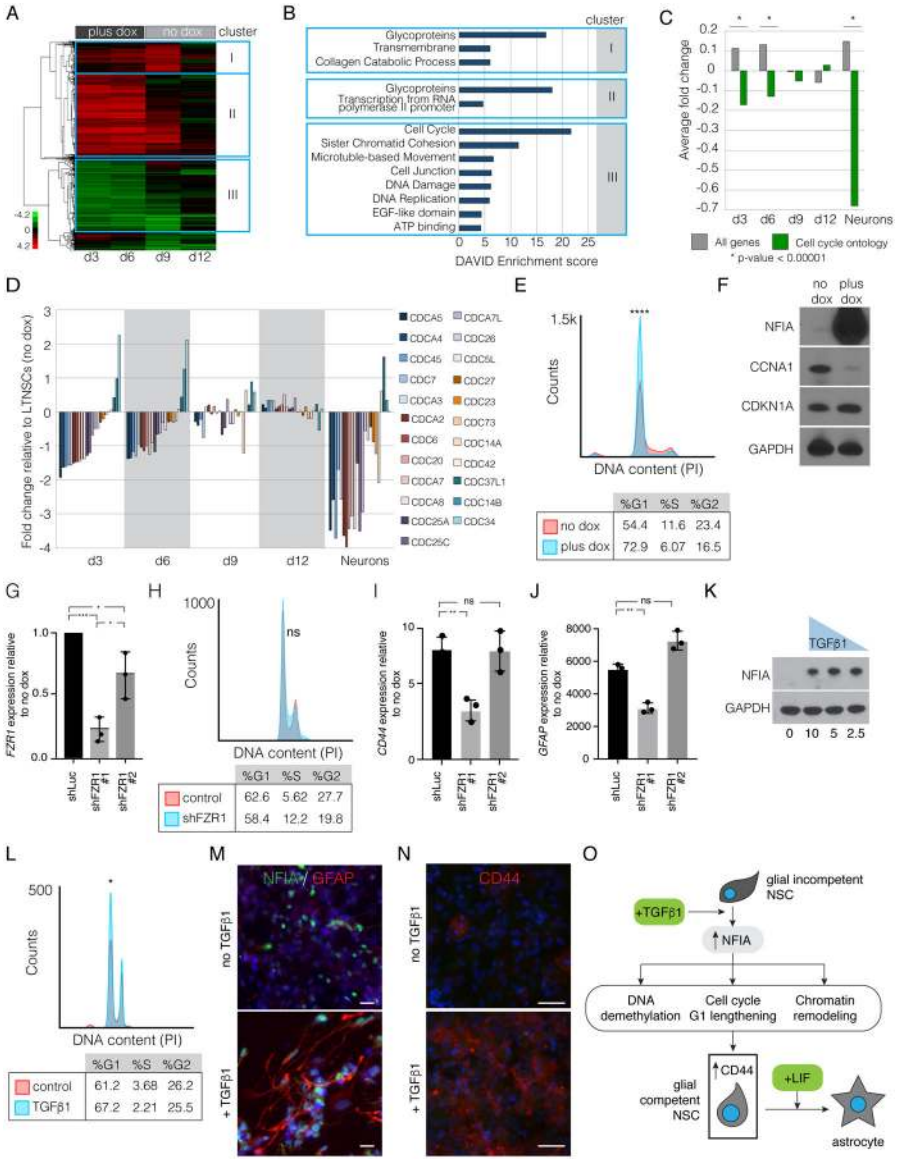


**Fig. 4. NFIA expression leads to a slower G1 cell cycle phase to induce glial competency.**

**A,** Unbiased hierarchical clustering of genes during the time course with three major clusters highlighted (Supplemental Table 2). **B**, Gene ontology analysis of the significant biological processes from each cluster represented in A. **C**, Global analysis of all genes and genes specifically in the cell cycle ontology (p-value < 0.000001 calculated using the hypergeometric distribution (n= a minimum of 3 biologically independent sequencing experiments). **D**, Graph of expression dynamics for all cell division cycle (CDC) genes during the time course. **E**, Cell cycle analysis by FACS on NSCs with or without dox for 7 days (n= 12 biologically independent experiments). One sided paired t-test on the G1 population with a ****p-value < 0.0001). **F**, Western blot analysis of CCNA1 and CDKN1A in LTNSCs with or without dox for 7 days (n= 3 biologically independent experiments). **G**, Quantitative PCR assessing the knockdown efficiency of shFZR1 in the presence of *NFIA* over expression (One way ANOVA, ***p-value < 0.0004, *p-value < 0.0185, n= 3

biological independent experiments). **H**, Analysis of the cell cycle phase with or without shRNA to FZR1. One sided paired t-test on the S phase population with a p-value < 0.07 (ns), n= 3 biological independent experiments. **I**, Quantitative PCR analysis of *CD44* expression in *NFIA* induced cells with or without shFZR1 (One way ANOVA, **p-value = 0.0055, n= 3 biological independent experiments). **J**, Quantitative PCR analysis of *GFAP* expression in *NFIA* induced cells similar to I but further induced with LIF (One way ANOVA, **p-value = 0.001, n= 3 biologically independent experiments). **K**, Western blot analysis of NFIA when induced with various levels of TGFβ1 for 7 days (n= 3 biologically independent experiments). **L**, Cell cycle analysis by FACS on NSCs treated with or without TGFβ1 for 48 hours (n= 3 biologically independent experiments). One sided paired t-test on the G1 cell cycle phase with a *p-value = 0.0386. **M**,Immunofluorescence staining for NFIA and GFAP on cultures treated with or without TGFβ1 for 14 days (n= 3 biologically independent experiments). **N**, Immunofluorescence staining for CD44 on cultures treated with or without TGFβ1 for 16 days (n= 3 biologically independent experiments). **O**, Model of NFIA-induced glial competency. Scale bars are 50 μm.